scientific reports

Check for updates

OPEN

Battery-less long-range wireless fluidic sensing system using flexible additive manufacturing ambient energy harvester and microfluidics

Tong-Hong Lin✉, Wenjing Su, Yepu Cui, Ryan Bahr & Manos M. Tentzeris

Fluid sensing has been an important but missing part of the massive Internet-of-Things sensor networks due to challenges including excessive manufacturing time/cost, finite wireless interrogation range, limited immunity to ambient clutter, and excessive required power for autonomous microfluidics operability. Here, we proposed an additive manufacturing flexible system as a solution to those challenges while enabling fluid analysis from controlled labs to virtually everywhere. Energy harvesting provides all required power for the actuation of the micro-pump enabling battery-less liquid sample acquisition. Energy sources including ultra-high-frequency radio frequency identification and hand-held devices like two-way talk radio are harvested simultaneously to support energy requirements for periodic monitoring every 6.6 min and on-demand monitoring within 4.63 s. Backscattering topologies are used to significantly extend the reading range while increasing the immunity to interferences and reducing the cost to the reader. A new additive manufacturing process is proposed to reduce fabrication time and cost while enabling massive scalability of flexible microfluidics. The good flexibility makes the system suitable for working toward future wearable applications. Prototypes of a sweat sensing system are demonstrated and successfully interrogated at 3 m with more than 15 dB signal-to-noise ratio using only a 14 dBm transmitter equivalent isotropic radiated power.

With the recent development of the Internet-of-Things (IoT), the increasing demand of large versatile sensor networks has facilitated the advancement of different sensors such as gas, heat, and vibration sensors. Furthermore, the integration of wearable and flexible sensors into IoT providing real-time biosensing/biomonitoring offers a huge advantage toward a safer and healthier life. However, fluid sensing remains a missing piece to the all-rounded sensor networks. Although, fluid analysis plays an important role in biochemical and environmental researches, most of them are still performed inside a lab. Therefore, a low-cost, autonomous (battery-free), wearable/flexible, and wireless fluid sensing system is required to elevating fluid analysis from lab to daily life.

Microfluidics will be the key to realize wearable and portable fluid analysis. The abilities to perform biochemical analysis with micro-scale liquid volumes, precise control of reaction, good repeatability, and high integrability with other circuits make microfluidic a great candidate to realize real-time wearable health and environmental monitoring and become a part of IoT networks[1–6]. Furthermore, by using functionalized micro-channels and electrodes, microfluidic can be extended to numerous applications including performing bio-monitoring such as sweat sensing[7], bio-analysis such as bacteria and virus detection[8], and personal medicine injection[9].

There are still major challenges which prevent microfluidic applications from ubiquitous daily use. One of the main challenges is the time and cost of manufacturing. A couple of currently used fabrication methods are glass etching for micro-channel, hot-embossing[10], and injecting molded plastic[4,11,12]. However, they are time consuming and not cost effective for massive production. Inkjet printing micro-channel has been proposed to reduce the cost by reducing the material used[13]. Nevertheless, the fabrication is time-consuming and it is hard to realize complex 3-dimensional (3D) structures. Another popular additive manufacturing (AM) techniques, 3D printing, has drawn a lot of attentions due to the low cost, fast prototyping, and the ability to realize complex 3D structures[5,13,14]. Nevertheless, there is still room for improvement especially when applying 3D printing and AM to flexible materials for wearable applications.

Electrical and Computer Engineering, Georgia Institute of Technology, Atlanta 30332-250, USA. ✉email: tlin97@gatech.edu

Another key challenge is wireless transmission of the sensing data. Most of previous works convert the bio-data into changes in resonance frequencies [15–19]. Although resonance type sensing can provide great sensitivity and accuracy, the data is read out by a Vector Network Analyzer (VNA) which is not suitable for wearable due to the bulky size of the VNA. There are some ways to wirelessly detect the resonance data but the range is very small and the accuracy is vulnerable to the environment clutters and multi-path reflections[20,21]. Thus, the reading ranges of these resonances type sensor are typically under 50 cm. The long reading range and immunity to clutter are especially important while applying microfluidic to IoT and smart city since hundreds and thousands of sensors are deployed at complicated environment. Therefore, both a novel method to modulate the bio-data and compatible wireless receiving and transmitting topologies which is long-range and accurate under complex environment are required.

The final challenge involves the power required to enable sufficient actuation force to move/sample liquids within micro-channels, especially in wearable platforms. Typical methods used are manually pressing fluids into the channels using syringes[22], using pumps[23] to press liquid, and using electrochemically controlled capillarity[7,24]. Although batteries like coin cells remain the easiest solution to drive the pump, the size, thickness, and weight make them hard to be integrated with other wearable and flexible components. The maintenance such as replace or recharge further increase the cost. Energy harvesting (EH) technologies harnessing surrounding energy provide great solutions to realize fully autonomous system[25–31]. Among different EH sources, electromagnetic (EM) waves which can be accessed all day at any locations are a great energy source candidate for EH[32–35]. Furthermore, the required circuits such as antenna can be seamlessly integrated with the wireless sensing system. However, there are drawbacks while harvesting EM waves. Far-field energy sources such as TV and communication signals are continuously available but low power density[36] while near-field energy sources such as smart phone and two-way talk radio support a much higher energy density but are accessible only short time[34].

In this work, a wearable and flexible fluidic sensing system is fabricated and analyzed. The fluidic sensing system is composed of three major parts: a microfluidic backscattering sensing system, a fluidic actuation system, and a battery-less power system. An AM fabrication process using both inkjet and 3D printing for flexible microfluidic sensor is proposed. The manufacturing process is fast and low cost with high accuracy and great 3D structural flexibility. The good reliability and repeatability is also demonstrated for potential massive production. Furthermore, the bio-measures from the microfluidic sensors are modulated using the conductivity of the fluid and transmitted by a long-range, high accuracy, and low power backscatter topology with great immunity to the environmental clutters. The battery-less power system driven by EH technology harvesting both far-field ultra-high frequency (UHF) radio-frequency identification (RFID) signals at 850–950 MHz and near-field two-way talk radio at 464.5 MHz is proposed to drive the micro-pump system and the wireless backscatter sensing system simultaneously. The far-field EM at lower power density is harvested continuously and fully charged the system every 5–10 min. Therefore, the far-field energy can be used to provide periodic monitoring. On the other hand, near-field higher power density EM is harvested and the bio-data can be retrieved in 5 s. Since the near-field energy can only be accessed while hand-held devices are in use, it is used to provide on-demand instantaneous measured results.

System architecture

The operation of the proposed battery-less long-range fluid sensor system is shown in Fig. 1a. The sensor system harvests energy from the Software-Defined radio (SDR) UHF RFID at 850–950 MHz and hand-held two-way talk radio at 464.5 MHz simultaneously for different user cases. The constantly broadcasting low-power far-field UHF RFID signal is used to keep powering the sensor system every couple of minutes for periodic bio-sensing. The hand-held devices such as smart phone or two-way talk radio is broadcasting only on-demand but at near-field. Thus, the harvested energy density is high and can trigger the sensing system in a couple of seconds for on-demand bio-sensing. The cheap SDR will also act as the receiver to receive the bio-sensing data. Furthermore, the reading range is long to reduce the required number of SDR in an IoT network.

The block diagram of the proposed battery-less sensor tag is shown in Fig. 1b and the conceptual prototype is shown in Fig. 1c. It is composed of a battery-less power system, a microfluidic backscattering sensing system, and a fludic actuation system. The battery-less power system is realized by utilizing EH techniques and used to drive the entire sensor system. The energy is harvested by the broadband planar monopole antenna and rectified into direct current (DC) energy through rectifier. The DC energy is then feed to the power management unit (PMU) to charge the super-capacitor. Once the charging stage is finished, the PMU will switch to discharge stage. At the discharge stage, the energy is used to drive the micro-pump control IC[37] to activate the micro-pump[38] and move the collected liquid into the microfluidic sensor. The above mentioned battery-less power system procedures are demonstrated as power flow in Fig. 1b. The microfluidic backscattering sensing system starts with modulating the bio-data into different resistances through the AM microfluidic sensor. The resistances are paralleled with a default resistor which is used to avoid open circuit while the mircro-channel is empty and captured by the EH-powered timer and modulated into voltage signals with different oscillating frequencies. The voltage signals are then used to control the switch and generate different switching frequency. The switching frequency will be modulated on the carrier frequency and send back to SDR through controlling the antenna loading impedance[39]. Once the signal is received, the modulated frequency can be converted to the resistance and then converted back to the bio-data. The microfluidic backscattering sensing system operation is demonstrated as the sensing signal flow in Fig. 1b. The fludic actuation system as the fluid flow shown in Fig. 1b moves the fluid into the microfluidic sensor.

The advantages and applications of the proposed sensor system is shown in Fig. 1d. The system is fully autonomous without any need for manually charging or replacing the battery. Furthermore, the battery-less micro-pump is used to provide a steady and reliable wearable fluid actuation force. A new AM process using

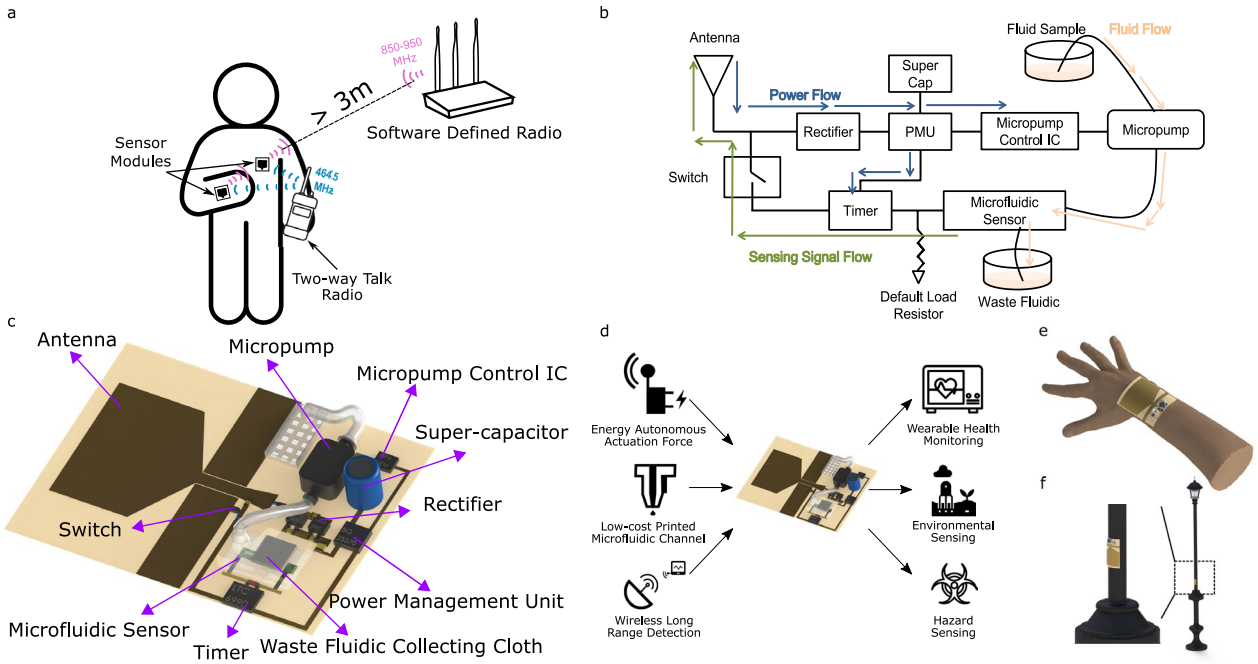

Figure 1. Battery-less long-range fluid sensor system architecture (**a**), The proposed battery-less sensor network which harvest energy from far-field UHF RFID and near-field two-way talk radio and transmit the bio-sensing data back to SDR. (**b**), the block diagram of the proposed battery-less sensor tag. (**c**), the conceptual prototype of the additive manufacturing flexible and wearable sensor tag. (**d**), the advantages and applications of the proposed sensor. (**e**), Wearable sweat sensing application. (**f**), environmental sensing of acid rain by deploying on the lamp post.

low-cost fast-prototyping inkjet and 3D printing is proposed to realize the microfluidic sensor. Instead of using resonances due to dielectric constant of the fluid, the backscatter system using conductivity of the fluid is adopted. The reading range is increased and the environment clutter impacts on the received signals are reduced. The applications of the proposed system are promising. Since the system is flexible, it can be used as wearable health monitoring such as sweat monitoring as shown in Fig. 1e. It can also be used for environmental sensing such as detecting the acid rain by deploying on the lamp post as shown in Fig. 1f. Finally, it can serve as hazard sensing by detecting the harmful substances inside liquid.

Atonomous (battery-less) power and actuation system

The battery-less power system is crucial to provide the energy requirement for wearable autonomous fluid actuation force and wireless interrogation. The energy harvesting circuit is composed of an antenna and a rectification circuit. As shown in Fig. 2a, the antenna used is an inkjet printed broadband monopole antenna on a flexible LCP material. The flexibility is also demonstrated by folding the antenna on the cylinder with 10.1 cm diameter as shown in Fig. 2b. The detailed inkjet printing process is in "Inkjet printing of battery-less power system" section. The measured S11 of the antenna under both flat and folded conditions are demonstrated in Fig. 2c. As shown in Fig. 2c, for the flat condition, S11 is smaller than − 10 dB from 700 MHz to over 1.2 GHz. On the other hand, the S11 is kept below − 9 dB from 850 MHz to over 1.2 GHz under folded condition. The UHF RFID band from 850 GHz to 950 GHz is fully covered on both conditions. For the far-field energy harvesting from UHF RFID reader, while the transmitted power is the maximum 36 dBm under FCC regulation, the measured received power by the broadband antenna at 900 MHz and 45 cm away is around 13 dBm. For the near-field energy harvesting, the measured coupling between the two-way talk radio antenna and the final output power at the output of the rectifier at is 21.5 dBm, 16.3 dBm, and 14.6 dBm while the distance is 5 cm, 10 cm, and 15 cm, respectively.

The rectification circuit diagram is shown in Fig. 2d. The matching circuit is composed of a 3.9 nH inductor and a tapered line. The length of the tapered line is 50 mm with a left-end width of 1.67 mm and a right-end width of 2.4 mm. The rectifier is composed of a two-stage charge pump using HSMS 282C Schottky diode from Avago[40]. The 270 pF capacitor is used to filter the higher order harmonics and the clean DC energy is feed to the PMU BQ 25570 from Texas Instrument[41]. The switch constructed by a SMP1340 pin diode from Skyworks[42] is mainly for the backscattering signal modulation which will be detailed in "Backscatter sensing system" section. The fabricated prototype using inkjet printing is shown in Fig. 2e. The measured input impedance from the tapered line is shown in Fig. 2f. As shown in Fig. 2f, while the switch is not driven (0 V), the matching is good enough for the RF signals to pass through. The other stage of the switch (3V) will be described in "Backscatter sensing system" section.

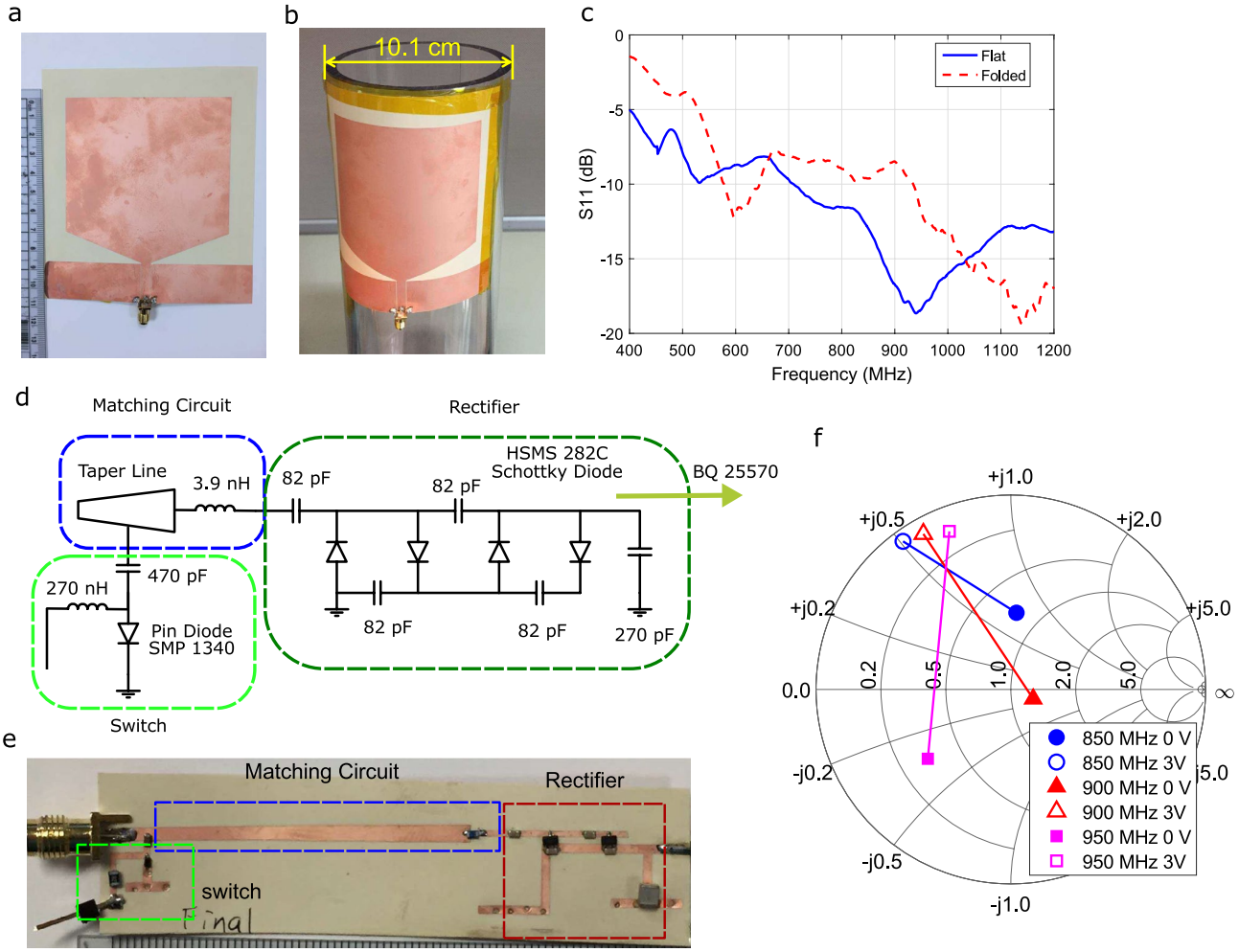

Figure 2. The energy harvesting system with backscatter controlling switch (**a**), the inkjet printed flexible broadband monopole antenna. (**b**), demonstration of the flexibility of the antenna. (**c**), the measured S11 of the antenna under flat and folded conditions. (**d**), the circuit diagram of the rectification circuit with backscatter signal controlling switch. (**e**), the photo of the fabricated prototype of the rectification circuit with backscatter signal controlling switch. (**f**), The measured input impedance of the circuit while the switch is powered with different voltages.

The rectification circuit shown in Fig. 2d is connected with the PMU circuit and super-capacitor. The measured RF-DC conversion efficiency of the rectifier while the load is the PMU is shown in Fig. 3a. Since larger power levels for near-field coupling at 464.5 MHz and lower power levels for far-field UHF RFID are expected, the rectification circuit is designed to have higher conversion efficiencies at expected power levels. As shown in Fig. 3a, the conversion efficiency of the large input power level (18 dBm) is higher around 464.5 MHz while the conversion efficiencies of the middle (10 dBm) and low (0 dBm) power levels are higher within UHF RFID frequency bands (850–950 MHz). Moreover, as shown in Fig. 3b, the flat and broadband conversion efficiency is realized within the entire UHF RFID bands.

The measured conversion efficiency under different input power is shown in Fig. 3c. As expected, higher conversion efficiency is realized under low and middle input power at the UHF RFID frequencies while high input power at the two-way talk radio frequency. In order to overcome the PMU cold-start frequency, the voltage has to be higher than 0.33 V[41]. From the measured results, the minimal required input power level for 464.5 MHz is 4 dBm. On the other hand, the minimal required input power level for UHF RFID frequencies is − 5 dBm which is about 3.5 m distance from SDR to the sensing system.

The output voltage of the PMU (Vout) and the voltage of the super-capacitor (VBAT) is shown in Fig. 3d. The PMU is programmed to switch to charging stage while VBAT is smaller than 3V and switch to discharging stage while VBAT reaches 5V. The output voltage of the PMU (Vout) which is used to power all applications is kept at 3V in discharging stage. The measured charging time is 4.63 s for near-field EH at 464.5 MHz with 20 dBm input power and 6.6 min for far-field EH at 900 MHz with 0 dBm input power. Therefore, near-field EH is suitable for on-demand quick monitoring and the continuous UHF RFID energy is suitable to provide periodic monitoring in 6.6 min. The battery-less power system is used to drive the piezo actuators inside the micro-pump

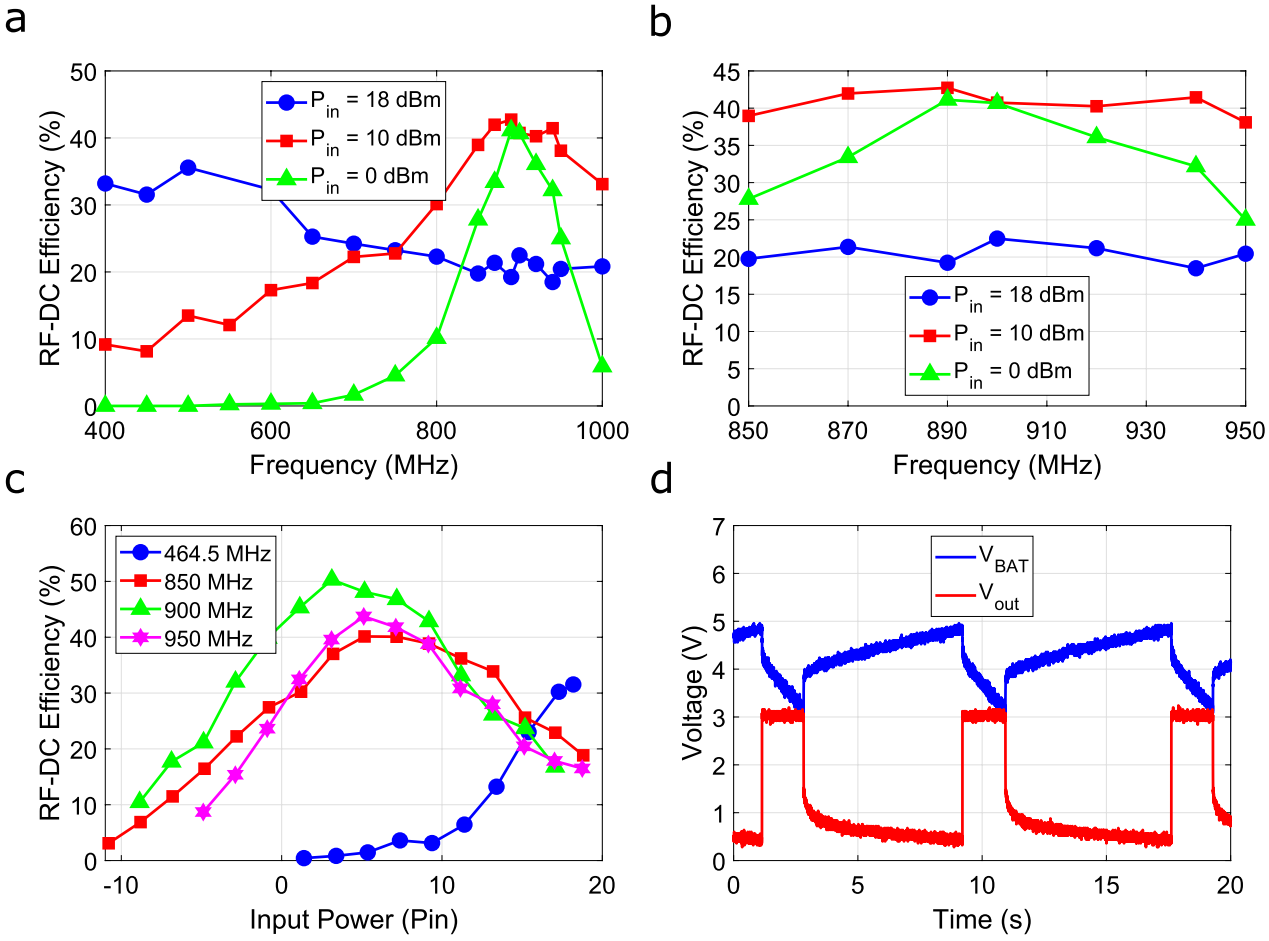

Figure 3. The harvested power characteristics of the batter-less power system. (**a**), The RF-DC conversion efficiency of the rectification circuit under three different input power levels. (**b**), The RF-DC conversion efficiency of the rectification circuit under three different input power levels within UHF RFID frequency range (850–950 MHz). (**c**), The RF-DC conversion efficiency of the rectification circuit under different input power levels. (**d**), The charging and discharging waveform at the output of the PMU.

with power consumption 150 mW. Thus, a fully autonomous fluid actuation force which is suitable for wearable and environment sensing is realized and expand the horizons of microfludic applications.

Backscatter sensing system

The backscatter topology is adopted due to the low power consumption and longer reading range with better immunity to the complex environment clutters. Once the micropump is activated and the fluid is pressed into the micro-channel, the resistance of the sensor will changed. As shown in Fig. 1b, the sensor is connected to the load of the timer LTC6990 from Aanlog Devices[43]. The timer is programmed to output a square wave with high voltage 3V and low voltage 0V. The frequency of the square wave is determined by the value of the load resistor which is the sensor in this case and the relation is as the following equation.

$$f_{out} = \frac{50\ \mathrm{k}\ \Omega}{R_{sensor}}\ \mathrm{MHz} \tag{1}$$

where the f_{out} is the output frequency of the square wave and R_{sensor} is the resistance of the sensor. The square wave is used to control the switch which is composed of a pin diode SMP 1340[42] and a LC feeding network as shown in Fig. 2d. The switch will alter the antenna load impedance as shown in Fig. 2f. As shown in Fig. 2f, while at 0V of the square wave, the antenna is connected to a relatively matched load. Therefore, the amplitude of the reflection wave is small. On the other hand, when the square wave is 3V, the reflection wave amplitude is large. The square wave frequency will be modulated to the carrier frequency of the reader by changing the amplitude of the reflection wave periodically. Since the modulated frequency is independent of the multi-path and clutter interferences, a much longer reading range is supported by the backscatter topology. Furthermore, the power consumption of this backscatter topology is smaller than 600 μW and is provided by the battery-less power system described in "Atonomous (battery-less) power and actuation system" section.

Proof-of-concept additive manufacturing microfluidic sweat sensor

The fabrication process of the fully AM microfluidic sensor is shown in Fig. 4a. Due to the high structural flexibility of the AM technologies, the fabrication process can be simplified into only three steps. Therefore, the prototyping time and cost can be reduced significantly. As shown in Fig. 4a, the first step is to 3D printing the microchannel. The second step is to inkjet printing the electrodes. The final step is to combine the electrodes and the microchannel. The detailed process and material handling are in "Inkjet and 3D printing of the sweat sensor" section. Since all substrate materials are flexible, good flexibility of the final microfluidic sensor can be realized. The fabrication process can be used to realize any microfluidic sensor and here a sweat sensor is used as a demonstration of the proposed fluidic sensing system. The liquid used to fill the micro-channel are 30.8 mmol/L and 71.9 mmol/L NaCl solutions to mimic low end and high end conductivity of human sweat[2].

The scalability is another critical aspect for manufacturing[44]. In order to test the stability and repeatability of the process, multiple prototypes are fabricated and the measured results are shown in Fig. 4b. The gap sizes between the two electrodes of all test prototypes are 13 mm. As shown in Fig. 4b, for the same test condition, the measured results of 4 samples are very close. Although the corner case might not be fully covered due to the small sample size, it can be estimated by using standard deviation while assuming normal distribution. Therefore, 1 standard deviation error bar is also included in Fig. 4b. The 95% confidence intervals for each test condition are 6.0, 4.9, 5.6, and 3.9 kΩ, respectively. The variations are within 20 kΩ under all conditions. As shown in Fig. 4b, the percentage of variation is smaller while the sensor resistance is larger which can be realized by increasing the electrode gap or reducing the microchannel diameter. The low process variation and the good repeatability of this process make it suitable for large-scale fabrication.

The final sweat sensor architecture is shown in Fig. 4c. The two silver nano-particle(SNP) electrodes are inkjet printed on PET with 30 mm gap between them. A layer of inkjet printed reactor such as carbon nanotubes or graphene-based thin film can be used to convert the concentration of the test substances such as ammonia into conductivity change[34,45]. Furthermore, functionalize electrodes can be used to perform bio-analysis such as detecting antibodies or bacteria[46,47] and further expand the future applications of the proposed fluid sensing system. Since the conductivity of human sweat will change based on different conditions, this layer of reactor is not needed in the sweat sensor. Finally, a 3D printed microfluidic channel is covered on the top of the electrodes with a 0.5 mm diameter. The 30 mm gap between electrodes and 0.5 mm diameter are used to make sure the microfluidic sensor resistances after filled with either 30.8 or 71.9 mmol/L NaCl solution can be sensed by the timer and generate switching frequency that is far enough to be distinguished wirelessly.

The fabricated prototype of the AM microfluidic sweat sensor is shown in Fig. 4d. The sensor is used as the load of the timer to control the oscillating frequency. A 667 kΩ resistor is paralleled with the microfluidic sweat sensor as the default resistance while the micro-channel is empty to avoid open-circuit loading to the timer. The 667 kΩ is chosen since it is large enough so that microfluidic sensor resistance is less impacted and small enough so that the timer can respond to. The sweat sensor is measured using a multimeter when 30.8 or 71.9 mmol/L NaCl artificial sweat is filled within the micro-channel. As shown in Fig. 4e, the resistances of the sweat

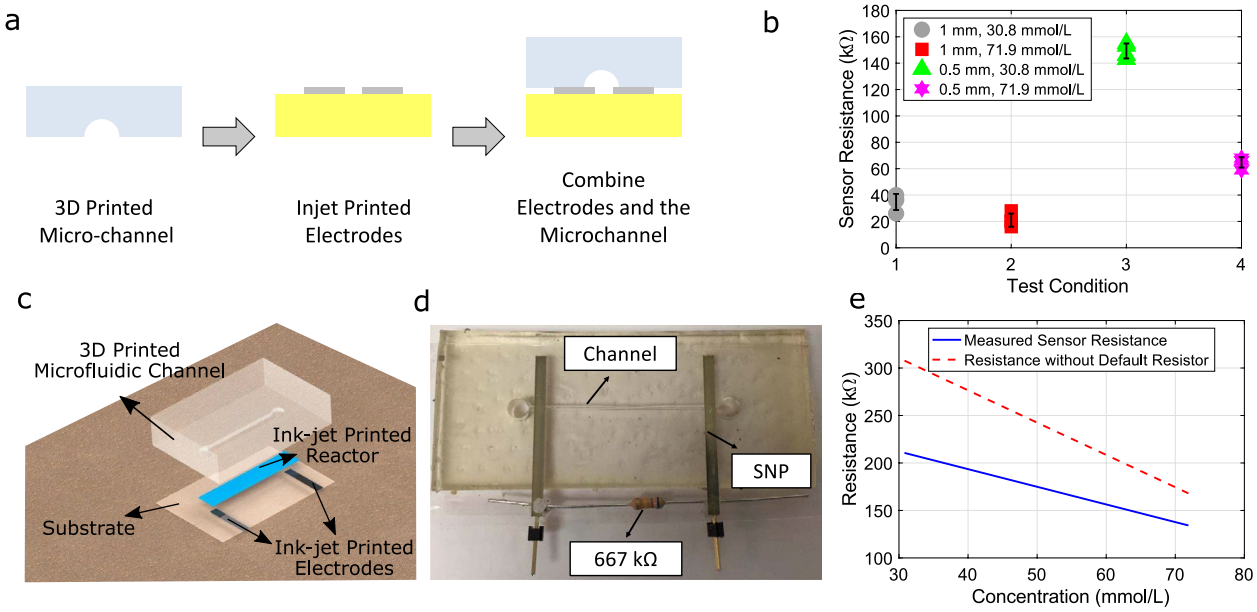

Figure 4. The prototype of the sweat sensor. (**a**), The fabrication process of a fully additive manufacturing microfluidic sweat sensor. (**b**), The measured repeatability and resistance of the additive manufacturing microfluidic sweat sensor without any additional parallel default resistor. (**c**), The architecture of the proposed fully additive manufacturing microfluidic sweat sensor. (**d**), The fabricated prototype of the additive manufacturing microfluidic sweat sensor. (**e**), The measured resistance of the sweat sensor prototype while filled with 30.8 mmol/L and 71.9 mmol/L NaCl artificial sweat. The calculated resistance without paralleling with a 667 kΩ default resistor is also included.

sensor are 211 kΩ and 134 kΩ when 30.8 and 70.1 mmol/L NaCl artificial sweat is filled inside the microchannel, respectively. Furthermore, the calculated resistance after excluding the parallel default 667 kΩ resistor is also included in Fig. 4e. Since the relationship between conductivity and concentration is roughly linear[2], the resistance of any intermediate concentration can be found by interpolation.

System field test

Each component of the proposed wireless fluidic sensing system is characterized and shown in Fig. 5a. The individual components are connected together based on the block diagram shown in Fig. 1b using SMA connectors for RF parts and jump wires for DC power supply. The antenna, rectifier, timer, super-cap array, and micropump control IC are fabricated using the same inkjet printing process on Ultralam 3850HT LCP substrate with a detailed description in "Inkjet printing of battery-less power system" section. Therefore, these components can be integrated seamlessly. The PMU BQ 25570 is the evaluation board (EVB) from Texas Instruments. The EVB is large since all functionalities are fan-out for testing and thus, the size can be reduced significantly and integrated with other components for future prototyping using the inkjet printing process on Ultralam 3850HT LCP substrate as shown in Fig. 1c. The microfluidic sensor fabricated by the process described in Fig. 4a and "Inkjet and 3D printing of the sweat sensor" section can be integrated with the rest components by gluing a piece of PET on the big Ultralam 3850HT LCP substrate and started the microfluidic sensor fabrication on the top of it.

The wireless measurement setup of the EH powered backscattering sensing system is shown in Fig. 5b. The signal generator is used to broadcast a 900 MHz carrier signal and the transmitted power is 12 dBm. The transmitted antenna is a 900 MHz monopole antenna and thus, the transmitted EIRP is around 14 dBm. The receiver is a spectrum analyzer with a monopole antenna. The signal generator and the spectrum analyzer can be replaced by a RFID reader or a cheaper SDR[34]. The two RFID reader antenna shown in Fig. 5b can be replaced with any UHF RFID antenna. The reading range is 3 m. The liquid moving speed of the micro-pump is 37.8 μL/s and the channel can be fully filled with 2.95 μL of liquid. Therefore, the microfluidic channel is fully filled and the data is sensed within 0.08 s.

The measured wireless backscattered results when the sweat sensor is filled with 30.8 and 71.9 mmol/L NaCl artificial sweat are shown in Fig. 5c and d, respectively. As shown in Fig. 5c, there are three spikes. The center one at 900 MHz is the carrier signal. The other two smaller spikes located at 232.9 kHz away from the carrier signal are the backscatter signals. The frequency separation between the carrier frequency and the backscatter frequency can be used to extract the fluidic concentration. From Eq. 1, the load resistance of the timer is 214.7 kΩ. which

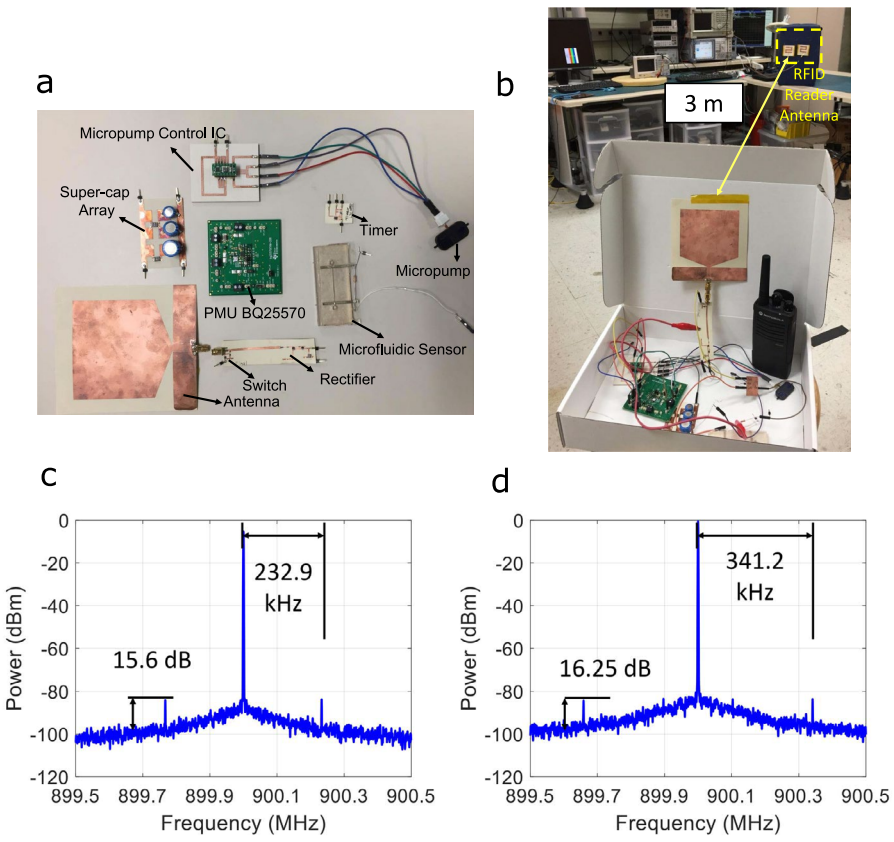

Figure 5. The wireless measurement of the proposed sensor system. (**a**), The prototype of each component. (**b**), the wireless measurement setup of the EH powered backscattering sensing system. (**c**), The measured wireless backscattered signals when the sweat sensor is filled with 30.8 mmol/L NaCl artificial sweat. (**d**), The measured wireless backscattered signals when the sweat sensor is filled with 71.9 mmol/L NaCl artificial sweat.

is very close to the measured results in Fig. 4e. Since there is a default 667 kΩ resistor as shown in Fig. 4d, the actual sensor resistance is 316.6 kΩ. The concentration of the sweat can be determined by the standard sensor resistance versus concentration table. As shown in Fig. 5d, the backscatter signals are 341.2 kHz away from the carrier frequency. The same procedure can be applied to find the load resistance of the timer which is 146.5 kΩ and is very close to the measured results in Fig. 4e. Furthermore, the difference between two concentrations of the solutions is 108.3 kHz which is large enough to be distinguished.

As shown in Fig. 5c and d, the signal-to-noise ratio (SNR) is 15.6 dB and 16.25 dB for two different concentrations. The FCC regulated maximum EIRP for UHF RFID is 36 dBm and SNR larger than 3 dB is typical larger enough to detect the signal. Thus, there is a 34.6 dB link budget can be used. From Friis equation, the reading range can be extended to 54.4 times which is 163 m if all link budget and hand-held EH source are used[34].

The comparison with previous works are summarized in Table 1. As shown in Table 1, in this work, fully AM including inkjet and 3D printing is utilized to provide not only 3D structure flexibility but also low cost and fast prototyping. Compared with other works, fluid actuation force provided by fully autonomous energy source is achieved in this work and open the potential to IoT applications. Furthermore, a much longer reading range is achieved due to the adoption of the backscatter topology and the proposed conductivity sensing. Compared with[48] utilizing change of resonance frequency due to dielectric constant change, a bulky VNA is not required to detect the bio-information. Controlled environment with absorber to reduced interference as in[50] is also not necessary due to the good interference resistant of the backscatter topology.

Conclusion

We have reported a new topology of an autonomous fluidic sensing system and an example of wearable and flexible sweat sensor. Solutions to multiple challenges including autonomous fluid actuation forces, extension of wireless reading range, and a low-cost microfluidic manufacturing method are proposed. The proposed system can potentially be a solution to perform fluid analysis outside the lab environment and introduce massive fluid sensing and fluid-related bio-sensing to the massive IoT sensor networks.

The wearable EH system harnessing UHF RFID from 850 to 950 MHz and hand-held two-way talk radio at 464.5 MHz simultaneously is proposed to power the entire system. Although the UHF RFID energy is low, it can be accessed constantly. The energy required to overcome the IC cold-start is − 5 dBm and thus, can be powered at 3.5 m away from the source. The bio-data can be read and send to the receiver every 6.6 min. On the other hand, the 464.5 MHz two-way talk radio can support high power due to the close proximity but only when the radio is on-used. The bio-data can be read and sent to the receiver in 4.63 s while using a 47 mF super-capacitor as energy storage device. The process can be even faster when a smaller super-capacitor is used. By utilizing both energy sources, the advantages of each resource are combined to support both periodical and on-demand bio-monitoring as well as reduce the maintenance cost of charging or replacing the batteries.

The entire sensor system is powered by the EH system. An energy autonomous micro-pump is used to press all kinds of liquid into the microfluidic sensors. Furthermore, the low-powered backscatter topology consuming only 600 μW is used to send sensor data wirelessly. Compared with previous works requiring a bulky and expansive VNA to detect the resonance frequency of the sensor, the backscatter topology can be wireless read with a cheap and small SDR. Moreover, a much longer reading range can be realized due to the good resist to multi-path interferences and clutters.

An AM process including inkjet and 3D printing is proposed to reduce the cost and fabrication time of the microfluidic sensor. The repeatability of the process is tested and the results are consistent with acceptable variations. A sweat sensor prototype is manufactured to demonstrate the manufacturing process. The conductivity change of the sensor is used as the test criteria since the backscatter topology is used. The artificial human sweat of concentration 30.8 mmol/L and 71.9 mmol/L using NaCl solutions are used to test the sweat sensor. The resistance while filled with 30.8 mmol/L and 71.9 mmol/L using NaCl solutions are 211 and 134 kΩ and the difference is large enough to be distinguished wirelessly.

The prototype of the entire sensor system is demonstrated. The system reading range is about 3 m under only 14 dBm EIRP. The backscatter signals at 232.9 kHz and 341.2 kHz away from the carrier frequency are detected successfully when sensors are filled with 30.8 mmol/L and 71.9 mmol/L NaCl solutions, respectively. The SNR ratio is above 15.6 dB. The reading range can be further extended to 163 m if the full 36 dBm EIRP, 3 dB SNR, and the hand-held EH source are used.

Work	Sensor fabrication	Fluid actuation/energy source	Wireless system	Freq	Reading range (m)
[48]	Micro-fabrication	Syringe/manual	NA	1.91 GHz	0
[20]	Inkjet printing	Syringe/manual	NFC	13.56 MHz	0.01
[21]	Etching+3D printing	Syringe pump/exterior power	Chipless RFID	2.9 GHz	0.24
[49]	Photolithography+laser pattern	Nature flow	Bluetooth	2.4 GHz	≈ 0.3
[50]	Inkjet printing	Syringe/manual	Passive RFID	1 GHz	0.5
This Work	Inkjet+3D printing	Micropump/energy harvest	Backscatter RFID	900 MHz	3

Table 1. Comparison with previous works about mircorfluidic sensors.

Methods

Inkjet printing of battery-less power system

The batter-less power system was fabricated by inkjet printing mask and etching. All the inkjet printing was done using Dimatix DMP-2831 inkjet printer. The substrate used was double-side copper-clad, Ultralam 3850HT LCP from Rogers Corporation. The substrate was first cleaned using acetone to remove dust. The mask pattern was printed using SU-8 polymer ink which was made by blending SU-8 2002 and SU-8 2005 from Microchem Corporation. The printed sample was soft baked at 95 °C on a hot plate for 5 min to evaporate the solvent within SU-8 ink. Then, it was cross-linked with a 600 mJ/cm^2 exposure of 365 nm UV light. Finally, it was hard baked under at 95 °C on a hot plate for 10 min. Once the mask was finished, the sample was submerged within $FeCl_3$ at 55 °C to etch the copper. Finally, acetone was used to strip the printed SU-8 mask from the board and expose the copper circuit. The components are then solder on the circuit sample.

Inkjet and 3D printing of the sweat sensor

The electrodes was first printed on PET substrate using SNP ink from Sun Chemical Corporation. Five layers of SNP ink were printed to reach acceptable conductivity. The drop-to-drop spacing is 20 μm and the inter-layer delay is 10 min with printing plate heated to 60 °C to make sure evaporation of solvent between layers. The sample then was put in convection oven at 180 °C for 60 min to evaporate the remaining solvent and sinter the SNP ink to form conductive traces. The micro-channel was 3D printed using Form3 stereolithography (SLA) 3D printer from Formlabs. A half-circle cylinder channel was 3D printed with flexible resin named Flexible 80A from Formlabs. The printed parts were then cleaned using Form wash filled with isopropyl alcohol (IPA) for 10 min. Then, the structure was further enhanced by Form cure at 60 °C for 15 min. The supporting materials were removed after the sample was cured. Finally, the electrodes and the microchannel were combined using Flexible 80A resin as glue. A thin layer of Flexible 80A resin was applied around the microchannel and then the PET and the 3D printed microchannel were pressed together and cured under UV light for 3 min. The default resistor was connected to the electrodes using conductive epoxy. The conductive epoxy was applied to the sample and placed on the hot plate at 120 °C for 15 min.

Design, characterization, and measurement

The system was design with the help of simulation software. The finite element method based full-wave EM simulation software High Frequency Structural Simulator (HFSS) from Ansoft is used to design the broadband monopole antenna. The harmonic balance function from Keysight Advanced Design System (ADS) was used to design and characterize the rectifier.

The antenna scattering parameter was measured using Anritsu 37369A VNA. For the field measurement shown in Fig. 5a, the signal generator is Rohde & Schwarz SMJ 100A and backscatter signals were captured using the the spectrum analyzer Tektronix RSA3408A.

Data availability

The datasets used and/or analysed during the current study are available from the corresponding author on reasonable request.

Received: 16 January 2024; Accepted: 25 July 2024
Published online: 01 August 2024

References

1. Entesari, K. & Saghati, A. P. Fluidics in microwave components. *IEEE Microw. Mag.* **17**, 50–75. https://doi.org/10.1109/MMM.2016.2538513 (2016).
2. Liu, G. *et al.* A wearable conductivity sensor for wireless real-time sweat monitoring. *Sens. Actuators B Chem.* **227**, 35–42. https://doi.org/10.1016/j.snb.2015.12.034 (2016).
3. Su, W., Cook, B. S. & Tentzeris, M. M. Additively manufactured microfluidics-based "peel-and-replace" RF sensors for wearable applications. *IEEE Trans. Microw. Theory Tech.* **64**, 1928–1936. https://doi.org/10.1109/TMTT.2016.2560177 (2016).
4. Mitchell, P. Microfluidics-downsizing large-scale biology. *Nat. Biotechnol.* **8**, 717–721. https://doi.org/10.1038/90754 (2001).
5. Weisgrab, G., Ovsianikov, A. & Costa, P. F. Functional 3D printing for microfluidic chips. *Adv. Mater. Technol.* **4**, 1900275. https://doi.org/10.1002/admt.201900275 (2019).
6. Pol, R., Céspedes, F., Gabriel, D. & Baeza, M. Microfluidic lab-on-a-chip platforms for environmental monitoring. *TrAC Trends Anal. Chem.* **95**, 62–68. https://doi.org/10.1016/j.trac.2017.08.001 (2017).
7. Nyein, H. Y. Y. *et al.* A wearable microfluidic sensing patch for dynamic sweat secretion analysis. *ACS Sens.* **3**, 944–952. https://doi.org/10.1021/acssensors.7b00961 (2018).
8. de Puig, H. *et al.* Minimally instrumented SHERLOCK (miSHERLOCK) for CRISPR-based point-of-care diagnosis of SARS-CoV-2 and emerging variants. *Sci. Adv.* **7**, eabh2944. https://doi.org/10.1126/sciadv.abh2944 (2021).
9. Babatain, W. *et al.* Expandable polymer assisted wearable personalized medicinal platform. *Adv. Mater. Technol.* **5**, 2000411. https://doi.org/10.1002/admt.202000411 (2020).
10. Qi, S. *et al.* Microfluidic devices fabricated in poly(methyl methacrylate) using hot-embossing with integrated sampling capillary and fiber optics for fluorescence detection. *Lab Chip* **2**, 88–95. https://doi.org/10.1039/B200370H (2002).
11. Attia, U. M., Marson, S. & Alcock, J. R. Micro-injection moulding of polymer microfluidic devices. *Microfluid. Nanofluid.* **7**, 1–28. https://doi.org/10.1007/s10404-009-0421-x (2009).
12. Wu, J. & Gu, M. Microfluidic sensing: State of the art fabrication and detection techniques. *J. Biomed. Opt.* **16**, 1–13. https://doi.org/10.1117/1.3607430 (2011).
13. Su, W., Cook, B. S., Fang, Y. & Tentzeris, M. M. Fully inkjet-printed microfluidics: A solution to low-cost rapid three-dimensional microfluidics fabrication with numerous electrical and sensing applications. *Sci. Rep.*https://doi.org/10.1038/srep35111 *(2016).*
14. Gross, B. C., Erkal, J. L., Lockwood, S. Y., Chen, C. & Spence, D. M. Evaluation of 3D printing and its potential impact on biotechnology and the chemical sciences. *Anal. Chem.* **86**, 3240–3253. https://doi.org/10.1021/ac403397r (2014).

15. Rocco, G. M. *et al.* 3-D printed microfluidic sensor in SIW technology for liquids' characterization. *IEEE Trans. Microw. Theory Tech.* **68**, 1175–1184. https://doi.org/10.1109/TMTT.2019.2953580 (2020).
16. Wiltshire, B. D. & Zarifi, M. H. 3-D printing microfluidic channels with embedded planar microwave resonators for RFID and liquid detection. *IEEE Microwave Wirel. Compon. Lett.* **29**, 65–67. https://doi.org/10.1109/LMWC.2018.2883715 (2019).
17. Govind, G. & Akhtar, M. J. Metamaterial-inspired microwave microfluidic sensor for glucose monitoring in aqueous solutions. *IEEE Sens. J.* **19**, 11900–11907. https://doi.org/10.1109/JSEN.2019.2938853 (2019).
18. Bao, X. *et al.* A planar one-port microwave microfluidic sensor for microliter liquids characterization. *IEEE J. Electromagn. RF Microw. Med. Biol.* **2**, 10–17. https://doi.org/10.1109/JERM.2018.2807984 (2018).
19. Mariotti, C., Su, W., Cook, B. S., Roselli, L. & Tentzeris, M. M. Development of low cost, wireless, inkjet printed microfluidic RF systems and devices for sensing or tunable electronics. *IEEE Sens. J.* **15**, 3156–3163. https://doi.org/10.1109/JSEN.2014.2374874 (2015).
20. Su, W. & Tentzeris, M. M. Smart test strips: Next-generation inkjet-printed wireless comprehensive liquid sensing platforms. *IEEE Trans. Ind. Electron.* **64**, 7359–7367. https://doi.org/10.1109/TIE.2017.2708022 (2017).
21. Wiltshire, B. D., Zarifi, T. & Zarifi, M. H. Passive split ring resonator tag configuration for RFID-based wireless permittivity sensing. *IEEE Sens. J.* **20**, 1904–1911. https://doi.org/10.1109/JSEN.2019.2950912 (2020).
22. Mumcu, G., Dey, A. & Palomo, T. Frequency-agile bandpass filters using liquid metal tunable broadside coupled split ring resonators. *IEEE Microw. Wirel. Compon. Lett.* **23**, 187–189. https://doi.org/10.1109/LMWC.2013.2247750 (2013).
23. Barrera, J. D. & Huff, G. H. A fluidic loading mechanism in a polarization reconfigurable antenna with a comparison to solid state approaches. *IEEE Trans. Antennas Propag.* **62**, 4008–4014. https://doi.org/10.1109/TAP.2014.2326422 (2014).
24. Wang, M., Trlica, C., Khan, M. R., Dickey, M. D. & Adams, J. J. A reconfigurable liquid metal antenna driven by electrochemically controlled capillarity. *J. Appl. Phys.* **117**, 194901. https://doi.org/10.1109/TAP.2014.2326422 (2015).
25. Harb, A. Energy harvesting: State-of-the-art. *Renew. Energy* **36**, 2641–2654. https://doi.org/10.1016/j.renene.2010.06.014 (2011).
26. Paradiso, J. & Starner, T. Energy scavenging for mobile and wireless electronics. *IEEE Pervasive Comput.* **4**, 18–27. https://doi.org/10.1109/MPRV.2005.9 (2005).
27. Taneja, J., Jeong, J. & Culler, D. Design, modeling, and capacity planning for micro-solar power sensor networks. In *2008 International Conference on Information Processing in Sensor Networks* (IPSN 2008), 407–418 https://doi.org/10.1109/IPSN.2008.67 (2008).
28. Carmo, J. P., Goncalves, L. M. & Correia, J. H. Thermoelectric microconverter for energy harvesting systems. *IEEE Trans. Ind. Electron.* **57**, 861–867. https://doi.org/10.1109/TIE.2009.2034686 (2010).
29. Bandodkar, A. J. *et al.* Sweat-activated biocompatible batteries for epidermal electronic and microfluidic systems. *Nat. Electron.* **3**, 554–562. https://doi.org/10.1038/s41928-020-0443-7 (2020).
30. Kulah, H. & Najafi, K. Energy scavenging from low-frequency vibrations by using frequency up-conversion for wireless sensor applications. *IEEE Sens. J.* **8**, 261–268. https://doi.org/10.1109/JSEN.2008.917125 (2008).
31. Garg, N. & Garg, R. Energy harvesting in iot devices: A survey. In *2017 International Conference on Intelligent Sustainable Systems (ICISS)*, 127–131 https://doi.org/10.1109/ISS1.2017.8389371 (2017).
32. Vyas, R. J., Cook, B. B., Kawahara, Y. & Tentzeris, M. M. E-wehp: A batteryless embedded sensor-platform wirelessly powered from ambient digital-tv signals. *IEEE Trans. Microw. Theory Tech.* **61**, 2491–2505. https://doi.org/10.1109/TMTT.2013.2258168 (2013).
33. Kim, S. *et al.* Ambient RF energy-harvesting technologies for self-sustainable standalone wireless sensor platforms. *Proc. IEEE* **102**, 1649–1666. https://doi.org/10.1109/JPROC.2014.2357031 (2014).
34. Lin, T.-H. *et al.* On-body long-range wireless backscattering sensing system using inkjet-/3-D-printed flexible ambient RF energy harvesters capable of simultaneous DC and harmonics generation. *IEEE Trans. Microw. Theory Tech.* **65**, 5389–5400. https://doi.org/10.1109/TMTT.2017.2768033 (2017).
35. Lin, T.-H., Su, W. & Tentzeris, M. M. Expand horizons of microfluidic systems: An inkjet printed flexible energy autonomous micropump system for wearable and IoT microfluidic applications. In *2018 IEEE/MTT-S International Microwave Symposium - IMS*, 812–815 https://doi.org/10.1109/MWSYM.2018.8439441 (2018).
36. Piñuela, M., Mitcheson, P. D. & Lucyszyn, S. Ambient RF energy harvesting in urban and semi-urban environments. *IEEE Trans. Microw. Theory Tech.* **61**, 2715–2726. https://doi.org/10.1109/TMTT.2013.2262687 (2013).
37. Bartels. mp6 series micropump electronics. https://www.bartels-mikrotechnik.de/wp-content/uploads/simple-file-list/EN/Manuals-and-Data-Sheets/mp6_electronics_Datasheet.pdf.
38. Bartels. mp6 series micropump. https://www.bartels-mikrotechnik.de/wp-content/uploads/simple-file-list/EN/Manuals-and-Data-Sheets/mp6_micropumps_Datasheet.pdf.
39. Kimionis, J., Georgiadis, A., Daskalakis, S. N. & Tentzeris, M. M. A printed millimetre-wave modulator and antenna array for backscatter communications at gigabit data rates. *Nat. Electron.* **4**, 439–446. https://doi.org/10.1038/s41928-021-00588-8 (2021).
40. Avago. Hsms-282x surface mount rf schottky barrier diodes. https://www.mouser.com/datasheet/2/678/avagotechnologies_AV02-1320EN,0-1217119.pdf.
41. Texas Instruments. Ultra low power harvester power management ic with boost charger, and nanopower buck converter. https://www.ti.com/product/BQ25570.
42. Skyworks. Fast switching speed, low capacitance, plastic packaged pin diodes. https://www.skyworksinc.com/-/media/SkyWorks/Documents/Products/101-200/SMP1340_Series_200051U.pdf.
43. Analog Devices. Timerblox: Voltage controlled silicon oscillator. https://www.analog.com/media/en/technical-documentation/data-sheets/LTC6990.pdf.
44. Saha, S. K. *et al.* Scalable submicrometer additive manufacturing. *Science* **366**, 105–109. https://doi.org/10.1126/science.aax8760 (2019).
45. Le, T. *et al.* Novel techniques for performance enhancement of inkjet-printed graphene-based thin films for wireless sensing platforms. In *2013 European Microwave Conference* 17–20 https://doi.org/10.23919/EuMC.2013.6686579 (2013).
46. Lynch, C. A., Eid, A., Fang, Y. & Tentzeris, M. M. Inkjet-/3D-/4D-printed "zero-power" flexible wearable wireless modules for smart biomonitoring and pathogen sensing. In *2021 IEEE International Conference on Flexible and Printable Sensors and Systems (FLEPS)* 1–3 https://doi.org/10.1109/FLEPS51544.2021.9469832 (2021).
47. Demuru, S., Marette, A., Kooli, W., Junier, P. & Briand, D. Flexible organic electrochemical transistor with functionalized inkjet-printed gold gate for bacteria sensing. In *2019 20th International Conference on Solid-State Sensors, Actuators and Microsystems & Eurosensors XXXIII (TRANSDUCERS & EUROSENSORS XXXIII)* 2519–2522 https://doi.org/10.1109/TRANSDUCERS.2019.8808309 (2019).
48. Ebrahimi, A., Scott, J. & Ghorbani, K. Ultrahigh-sensitivity microwave sensor for microfluidic complex permittivity measurement. *IEEE Trans. Microw. Theory Tech.* **67**, 4269–4277. https://doi.org/10.1109/TMTT.2019.2932737 (2019).
49. Song, Y. *et al.* Wireless battery-free wearable sweat sensor powered by human motion. *Sci. Adv.* **6**, eaay9842. https://doi.org/10.1126/sciadv.aay9842 (2020).
50. Cook, B. S., Cooper, J. R. & Tentzeris, M. M. An inkjet-printed microfluidic RFID-enabled platform for wireless lab-on-chip applications. *IEEE Trans. Microw. Theory Tech.* **61**, 4714–4723. https://doi.org/10.1109/TMTT.2013.2287478 (2013).

Author contributions

T.L., W.S. and M.M.T. conceived the experiments; T.L. conducted the experiments and analyzed the results; T.L. and Y.C. fabricated the devices; T.L. and Y.C. structurally characterized the devices; T.L., R.B. and M.M.T. drafted the main manuscript; all authors reviewed the manuscript.

Competing interests

The authors declare no competing interests.

Additional information

Correspondence and requests for materials should be addressed to T.-H.L.

Reprints and permissions information is available at www.nature.com/reprints.

Publisher's note Springer Nature remains neutral with regard to jurisdictional claims in published maps and institutional affiliations.